# The True Role of Accelerometer Feedback in Quadrotor Control

Philippe Martin, Erwan Salaun

# The True Role of Accelerometer Feedback in Quadrotor Control

Philippe Martin and Erwan Salaün

*Abstract*— A revisited quadrotor model is proposed, including in particular the so-called rotor drag. It is different from the traditionally considered model, even at first order, and much better explains the role of accelerometer feedback in control algorithms. The theoretical derivation is supported by experimental data.

## I. INTRODUCTION

Quadrotor control has been an active area of investigation for several years. On the one hand the quadrotor has several qualities, among them its very simple mechanical design, and qualifies as a viable concept of mini Unmanned Aerial Vehicle (UAV) for real-life missions; on the other hand it is perceived in the control community as a very rich case study in theoretical and applied control. The first control objective is to ensure a stable flight at moderate velocities and in particular in hovering; this fundamental building block is then used to develop higher-level tasks (e.g. autonomous flight including waypoint following, obstacle avoidance, automatic take off and landing, etc.).

Putting aside purely control-theoretic works focused on the detailed analysis of control laws without real-world sensors in mind, as well as experiments designed to work only in the laboratory with an off-board measuring device (e.g. [1] use an electromagnetic motion tracking system[1], with very short range), real quadrotor designs all rely at the heart on strapdown MEMS inertial sensors (gyroscopes and accelerometers). Such sensors are also used in "preliminary" experiments where the quadrotor is tethered to a test rig and free only to rotate [2], [3], [4]. These inertial sensors may be used alone (as far as horizontal stabilization is concerned) [5], or supplemented by other sensors which provide usually some position-related information. Representative designs are: 3 ultrasonic rangers [6]; a (simple) GPS module when outdoors and 4 infrared rangers when indoors [7]; a carrier phase differential GPS [8]; a vision system [9], [10]. Since these extra sensors have inherent drawbacks (low bandwidth, possible temporary unavailability, etc.), inertial sensors remain essential for basic stabilization.

Nearly all the above-mentioned works rely on essentially the same physical model: only aerodynamic forces and moments proportional to the square of the propellers angular velocities are explicitly taken into account. Other aerodynamics effects are omitted and considered as unmodeled



Fig. 1.   Our home-built quadrotor: the "Quadricopter".

disturbances to be rejected by the control law. The alleged reason is that these effects are proportional to the square of the quadrotor linear velocity [11], hence very small near hovering. Few authors explicitly consider other aerodynamic effects: [4] consider aerodynamic stability derivatives, but draw no clear-cut conclusion about their importance; [12], [13] consider without physical motivations aerodynamic effects linear w.r.t. the quadrotor linear and angular velocities, but propose negligible numerical values; [8] judge them negligible at low velocities, and focus on nonlinear aspects at moderate velocities; [14] physically motivates the presence of effects nearly linear w.r.t the quadrotor linear and angular velocities, but provide no experimental data and are concerned only with the open-loop system.

As for accelerometers, they are usually considered as giving approximately the components of gravity in body axes, under the assumption that the quadrotor linear acceleration is small. Accordingly, the pitch and roll angles are estimated from gyroscope and accelorometer measurements thanks to some sensor fusion algorithm: Extended Kalman Filter (EKF) [2]; complementary filter, linear [3], [7] or nonlinear [10] (see [15], [16], [17] for an account of such nonlinear filters and related nonlinear observers); unspecified algorithm [5], [9]. Commercial "attitude sensors" such as the 3DM-GX[2] used in [6] run exactly on the same principles, with some sort of EKF. Recall that MEMS inertial sensors are not accurate enough for "true" Schuler-based inertial navigation, see e.g. [18, chap. 5] for details.

With so many theoretical and experimental works, one could think there is little more to say about such a basic issue as linear control around hovering with inertial sensors. This

Ph. Martin is with Centre Automatique et Systèmes, MINES ParisTech, Paris, France `philippe.martin@mines-paristech.fr`

E. Salaün is with Decision and Control Laboratory, School of Aerospace Engineering, Georgia Institute of Technology, Atlanta GA 30332-0150, USA `erwan.salaun@gatech.edu`

[1] www.polhemus.com

[2] www.microstrain.com

paper nevertheless supports a different opinion: the traditional analysis is not quite correct, even at first order. Indeed aerodynamics effects proportional to the propeller angular velocity times the quadrotor linear or angular velocity do appear at first order. In particular the so-called rotor drag must be considered to correctly account for the accelerometer measurements

The paper is organized as follows: in section II a "revisited" model of the quadrotor with inertial measurements is derived; in section III its main features are experimentally validated; finally section IV discusses its implications on control schemes.

## II. REVISITED QUADROTOR MODEL

### A. Model of a single propeller near hovering

We first consider a single propeller rotating with angular velocity $\varepsilon_i \omega_i$ around its axis $\vec{k}_b$; $\omega_i$ is positive, with $\varepsilon_i = 1$ (resp. $-1$) for counterclockwise (resp. clockwise) rotation. The geometric center $A_i$ of the propeller moves with a given velocity $\vec{V}_{A_i}$ while the rotor plane (by definition perpendicular to $\vec{k}_b$) undergoes angular velocity $\vec{\Omega}$; the total angular velocity of the propeller is thus $\vec{\Omega} + \varepsilon_i \omega_i \vec{k}_b$. Following e.g. [19], the aerodynamic efforts on the propeller resolve into the force $\vec{F}_i$ and moment $\vec{M}_i$ at $A_i$,

$$\vec{F}_i = -a\omega_i^2 \vec{k}_b - \omega_i \left( \lambda_1 \vec{V}_{A_i}^\perp - \lambda_2 \vec{\Omega} \times \vec{k}_b \right)$$
$$+ \varepsilon_i \omega_i \left( \lambda_3 \vec{V}_{A_i} \times \vec{k}_b - \lambda_4 \vec{\Omega}^\perp \right) \quad (1)$$

$$\vec{M}_i = -b\varepsilon_i \omega_i^2 \vec{k}_b - \omega_i \left( \mu_1 \vec{V}_{A_i}^\perp + \mu_2 \vec{\Omega} \times \vec{k}_b \right)$$
$$- \varepsilon_i \omega_i \left( \mu_3 \vec{V}_{A_i} \times \vec{k}_b + \mu_4 \vec{\Omega}^\perp \right), \quad (2)$$

where $a$, $b$, the $\lambda_i$'s and $\mu_i$'s are positive constants; the projection of a vector $\vec{u}$ on the rotor plane is

$$\vec{u}^\perp := \vec{k}_b \times \left( \vec{u} \times \vec{k}_b \right) = \vec{u} - \left( \vec{u} \cdot \vec{k}_b \right) \vec{k}_b.$$

The above relations rely on classical blade element theory, with two extra simplifications, and (approximately) apply to any propeller, rigid or not:

- higher-order terms in linear and angular velocities have been neglected. This is valid near hovering, i.e. for small $\vec{V}_{A_i}$ and $\vec{\Omega}$. Here $\vec{V}_{A_i}$ "small" means small with respect to the propeller tip speed (about $40m/s$ in our case), so that $5m/s$ can be considered small
- linear and angular accelerations have been neglected. Their contribution is small since the mass of the propeller is in our case very small with respect to the total mass of the quadrotor.

The velocities in the previous equations are of course velocities with respect to the air stream, not with respect to the ground. They coincide when there is no wind, which we assume in the sequel.

The term $\omega_i \lambda_1 \vec{V}_{A_i}^\perp$ in (1) is often called *H-force* or *rotor drag* in the helicopter literature. Also notice the simplified expressions (1)-(2), though directly based on textbook aerodynamics, do not seem to appear in the literature under this compact form very handy for control purposes.
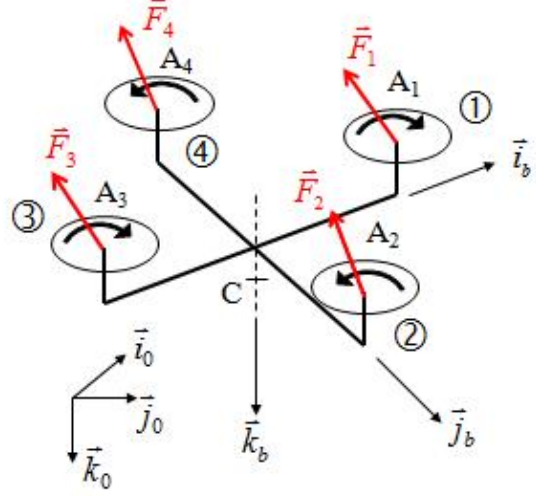


Fig. 2. Sketch of the complete quadrotor.

### B. Model of the complete quadrotor

The quadrotor consists of a rigid frame with four propellers (directly) driven by electric motors, see figure 2. The structure is symmetrically arranged, with one pair of facing propellers rotating clockwise and the other pair counterclockwise. The four propellers have the same axis $\vec{k}_b$; $\vec{i}_b := \frac{\vec{A_3 A_1}}{\|\vec{A_3 A_1}\|}$, $\vec{j}_b := \frac{\vec{A_4 A_2}}{\|\vec{A_4 A_2}\|}$ and $\vec{k}_b$ then form a direct coordinate frame. Let $A$ be the geometric center of the $A_i$'s and $l := \frac{1}{2}\|\vec{A_3 A_1}\| = \frac{1}{2}\|\vec{A_2 A_4}\|$; clearly, $\sum_{i=1}^4 \vec{AA_i} = 0$.

The whole system $\mathcal{B}$, with mass $m$ and center of mass $C$, thus involves five rigid bodies: the frame/stators assembly $\mathcal{B}_0$ and the four propeller/motor assemblies $\mathcal{B}_i$; clearly, $\vec{CA} = h\vec{k}_b$ for some (signed) length $h$. Resolved in the $(\vec{i}_b, \vec{j}_b, \vec{k}_b)$ frame, the velocity of $C$ reads $\vec{V}_C = u\vec{i}_b + v\vec{j}_b + w\vec{k}_b$ and the angular velocity of $\mathcal{B}_0$ reads $\vec{\Omega} = p\vec{i}_b + q\vec{j}_b + r\vec{k}_b$.

We assume the only efforts acting on $\mathcal{B}$ are the weight and the aerodynamic efforts created by the propellers as described in the previous section. In particular we neglect the drag created by the frame, which is quadratic with respect to the velocity, hence small at low velocities. Newton's laws for the whole system then read

$$m\dot{\vec{V}}_C = m\vec{g} + \sum_{i=1}^4 \vec{F}_i \quad (3)$$

$$\dot{\vec{\sigma}}_C^\mathcal{B} = \sum_{i=1}^4 \vec{CA_i} \times \vec{F}_i + \vec{M}_i, \quad (4)$$

where $\vec{\sigma}_C^\mathcal{B} = \int_\mathcal{B} \vec{CM} \times \dot{\vec{CM}} d\mu(M)$ is the kinetic momentum of $\mathcal{B}$.

In hovering $\vec{V}_C$ and $\vec{\Omega}$, hence $\vec{V}_{A_i}$ are zero; from (1)–(4), see also (6)-(7), this implies $a(\omega_1^2 + \omega_2^2 + \omega_3^2 + \omega_4^2) = g$ and $\omega_1^2 - \omega_2^2 + \omega_3^2 - \omega_4^2 = \omega_1^2 - \omega_3^2 = \omega_2^2 - \omega_4^2 = 0$, hence $\omega_i = \bar{\omega} := \sqrt{\frac{mg}{4a}}$.

For each $\mathcal{B}_i$, we can also write

$$\dot{\vec{\sigma}}_{A_i}^{\mathcal{B}_i} \cdot \vec{k}_b = \vec{M}_i \cdot \vec{k}_b + \varepsilon_i \Gamma_i, \quad (5)$$

where $\vec{\sigma}_{A_i}^{\mathcal{B}_i} = \int_{\mathcal{B}_i} A_i\vec{M} \times A_i\dot{\vec{M}} d\mu(M)$ is the kinetic momentum of $\mathcal{B}_i$, and $\Gamma_i$ is the (positive) torque created by the motor. For simplicity we have considered $A_i$ as the center of mass of $\mathcal{B}_i$ (in fact the two points are slightly apart). We also consider the $\Gamma_i$'s as the control inputs (it is nevertheless easy to include the behavior of the electric motors both for modeling and control).

We now evaluate the right-handsides of (3)-(4)-(5). Since

$$\vec{V}_{A_i} = \vec{V}_C + \dot{\vec{CA}} + \dot{\vec{AA_i}}$$
$$= \vec{V}_C + h\vec{\Omega} \times \vec{k}_b + \vec{\Omega} \times \vec{AA_i},$$

we find

$$\lambda_1 \vec{V}_{A_i}^{\perp} - \lambda_2 \vec{\Omega} \times \vec{k}_b$$
$$= \lambda_1 \left( \vec{V}_C^{\perp} + \left(h\vec{\Omega} \times \vec{k}_b\right)^{\perp} + \left(\vec{\Omega} \times \vec{AA_i}\right)^{\perp} \right) - \lambda_2 \vec{\Omega} \times \vec{k}_b$$
$$= \lambda_1 \vec{V}_C^{\perp} - \lambda_2' \vec{\Omega} \times \vec{k}_b - r\lambda_1 \vec{AA_i} \times \vec{k}_b$$
$$\lambda_3 \vec{V}_{A_i} \times \vec{k}_b - \lambda_4 \vec{\Omega}^{\perp}$$
$$= \lambda_3 \left( \vec{V}_C + h\vec{\Omega} \times \vec{k}_b + \vec{\Omega} \times \vec{AA_i} \right) \times \vec{k}_b - \lambda_4 \vec{\Omega}^{\perp}$$
$$= \lambda_3 \vec{V}_C \times \vec{k}_b + \lambda_4' \vec{\Omega}^{\perp} + r\lambda_3 \vec{AA_i}.$$

We have used the fact that $\vec{AA_i}$ is colinear to either $\vec{\imath}_b$ or $\vec{\jmath}_b$, and set $\lambda_2' =: \lambda_2 - h\lambda_1$ and $\lambda_4' := \lambda_4 + h\lambda_3$. Therefore,

$$\sum_{i=1}^{4} \vec{F}_i = -a \left(\sum_{i=1}^{4}\omega_i^2\right) \vec{k}_b - \left(\sum_{i=1}^{4}\omega_i\right)\left(\lambda_1\vec{V}_C^{\perp} - \lambda_2'\vec{\Omega} \times \vec{k}_b\right)$$
$$+ \left(\sum_{i=1}^{4}\varepsilon_i\omega_i\right)\left(\lambda_3\vec{V}_C \times \vec{k}_b - \lambda_4'\vec{\Omega}^{\perp}\right)$$
$$+ r\lambda_1 \left(\sum_{i=1}^{4}\omega_i\vec{AA_i}\right) \times \vec{k}_b + r\lambda_3 \left(\sum_{i=1}^{4}\varepsilon_i\omega_i\vec{AA_i}\right).$$

Notice the last two lines contain only second order terms: indeed, $\vec{\Omega}$, $\vec{V}_C$, $\sum_{i=1}^{4}\varepsilon_i\omega_i$, $\sum_{i=1}^{4}\omega_i\vec{AA_i}$ and $\sum_{i=1}^{4}\varepsilon_i\omega_i\vec{AA_i}$ all vanish in hovering. Neglecting these terms, we have

$$\sum_{i=1}^{4} \vec{F}_i \approx -a \left(\sum_{i=1}^{4}\omega_i^2\right) \vec{k}_b - \left(\sum_{i=1}^{4}\omega_i\right)\left(\lambda_1\vec{V}_C^{\perp} - \lambda_2'\vec{\Omega} \times \vec{k}_b\right).$$

Likewise,

$$\sum_{i=1}^{4} \vec{CA} \times \vec{F}_i + \vec{AA_i} \times \vec{F}_i + \vec{M}_i$$
$$\approx -a \left(\sum_{i=1}^{4}\omega_i^2\vec{AA_i}\right) \times \vec{k}_b - b\left(\sum_{i=1}^{4}\varepsilon_i\omega_i^2\right)\vec{k}_b$$
$$- r\lambda_1 l^2 \left(\sum_{i=1}^{4}\omega_i\right)\vec{k}_b - \left(\sum_{i=1}^{4}\omega_i\right)\left(\mu_1'\vec{V}_C \times \vec{k}_b + \mu_2'\vec{\Omega}^{\perp}\right),$$

where $\mu_1' := \mu_1 - h\lambda_1$, $\mu_2' := \mu_2 - h\mu_1$ and $\mu_2'' := \mu_2' - h\lambda_2$.

A further simplification, valid for a rather rigid propeller, is to consider that $\lambda_2'$ is zero. Indeed $h$ is by design small, and for a rather rigid propeller so is $\lambda_2$. This yields

$$\sum_{i=1}^{4} \vec{F}_i \approx -a \left(\sum_{i=1}^{4}\omega_i^2\right) \vec{k}_b - \lambda_1 \left(\sum_{i=1}^{4}\omega_i\right)\vec{V}_C^{\perp}.$$

Gathering the previous computations, (3)-(4)-(5) now read

$$m\dot{\vec{V}}_C = m\vec{g} - a\left(\omega_1^2 + \omega_2^2 + \omega_3^2 + \omega_4^2\right)\vec{k}_b$$
$$- \lambda_1(\omega_1 + \omega_2 + \omega_3 + \omega_4)\vec{V}_C^{\perp} \quad (6)$$
$$\dot{\vec{\sigma}}_C^{\mathcal{B}} = -b\left(\omega_1^2 - \omega_2^2 + \omega_3^2 - \omega_4^2\right)\vec{k}_b$$
$$+ al(\omega_1^2 - \omega_3^2)\vec{\jmath}_b - al(\omega_2^2 - \omega_4^2)\vec{\imath}_b$$
$$- (\omega_1 + \omega_2 + \omega_3 + \omega_4)\left(\mu_1'\vec{V}_C \times \vec{k}_b + \mu_2''\vec{\Omega}^{\perp}\right)$$
$$- r\lambda_1 l^2(\omega_1 + \omega_2 + \omega_3 + \omega_4)\vec{k}_b \quad (7)$$
$$\dot{\vec{\sigma}}_{A_i}^{\mathcal{B}_i} \cdot \vec{k}_b = \varepsilon_i(\Gamma_i - b\omega_i^2). \quad (8)$$

We then evaluate the left-handsides of (3)-(4)-(5). The approach is fairly standard.

$$\vec{\sigma}_C^{\mathcal{B}} = \int_{\mathcal{B}} C\vec{M} \times C\dot{\vec{M}} d\mu(M)$$
$$= \int_{\mathcal{B}_0} C\vec{M} \times C\dot{\vec{M}} d\mu(M)$$
$$+ \sum_{i=1}^{4} \int_{\mathcal{B}_i} C\vec{M} \times \left(C\dot{\vec{A}}_i + A_i\dot{\vec{M}}\right) d\mu(M)$$
$$= \int_{\mathcal{B}_0} C\vec{M} \times \left(\vec{\Omega} \times C\vec{M}\right) d\mu(M) + \sum_{i=1}^{4} \int_{\mathcal{B}_i} C\vec{M} \times$$
$$\left(\vec{\Omega} \times C\vec{A}_i + (\vec{\Omega} + \varepsilon_i\omega_i\vec{k}_b) \times A_i\vec{M}\right) d\mu(M)$$
$$= \int_{\mathcal{B}} C\vec{M} \times \left(\vec{\Omega} \times C\vec{M}\right) d\mu(M)$$
$$+ \sum_{i=1}^{4} \int_{\mathcal{B}_i} A_i\vec{M} \times \left(\varepsilon_i\omega_i\vec{k}_b \times A_i\vec{M}\right) d\mu(M)$$
$$= \mathcal{I}_C^{\mathcal{B}} \cdot \vec{\Omega} + \sum_{i=1}^{4}\varepsilon_i\omega_i\left(\mathcal{I}_{A_i}^{\mathcal{B}_i} \cdot \vec{k}_b\right)$$
$$= Ip\vec{\imath}_b + Iq\vec{\jmath}_b + \left(Jr + J_r\sum_{i=1}^{4}\varepsilon_i\omega_i\right)\vec{k}_b,$$

where $I, J, J_r$ are strictly positive constants. In the last equation we replaced in the computation of the inertia tensors $\mathcal{I}^{\mathcal{B}}, \mathcal{I}_{A_i}^{\mathcal{B}_i}$ the actual propellers by disks with the same masses and radii, and took advantage of the various symmetries; this "averaging" approximation is justified by the fact that the propeller angles vary much faster than all the other kinematic variables (besides this approximation is already heavily used in the blade element theory used to derive (1)-(2)).

Using the same approximation,

$$\vec{\sigma}_{A_i}^{\mathcal{B}_i} = \int_{\mathcal{B}_i} A_i\vec{M} \times A_i\dot{\vec{M}} d\mu(M)$$
$$= \int_{\mathcal{B}_i} A_i\vec{M} \times \left((\vec{\Omega} + \varepsilon_i\omega_i\vec{k}_b) \times A_i\vec{M}\right) d\mu(M)$$
$$= \mathcal{I}_{A_i}^{\mathcal{B}_i} \cdot (\vec{\Omega} + \varepsilon_i\omega_i\vec{k}_b)$$
$$= I_r p\vec{\imath}_b + I_r q\vec{\jmath}_b + J_r(r + \varepsilon_i\omega_i)\vec{k}_b,$$

where $I_r$ is a strictly positive constant.

Eventually,

$$
\begin{pmatrix} \dot{\vec{V}}_C \cdot \vec{\imath}_b \\ \dot{\vec{V}}_C \cdot \vec{\jmath}_b \\ \dot{\vec{V}}_C \cdot \vec{k}_b \end{pmatrix} = \begin{pmatrix} \dot{u} + qw - rv \\ \dot{v} + ru - pw \\ \dot{w} + pv - qu \end{pmatrix} \tag{9}
$$

$$
\begin{pmatrix} \dot{\vec{\sigma}}_C^{\mathcal{B}} \cdot \vec{\imath}_b \\ \dot{\vec{\sigma}}_C^{\mathcal{B}} \cdot \vec{\jmath}_b \\ \dot{\vec{\sigma}}_C^{\mathcal{B}} \cdot \vec{k}_b \end{pmatrix} = \begin{pmatrix} I\dot{p} + (J - I)qr + J_r q \sum_{i=1}^4 \varepsilon_i \omega_i \\ I\dot{q} - (J - I)pr - J_r p \sum_{i=1}^4 \varepsilon_i \omega_i \\ J\dot{r} + J_r \sum_{i=1}^4 \varepsilon_i \dot{\omega}_i \end{pmatrix} \tag{10}
$$

$$
\dot{\vec{\sigma}}_{A_i}^{\mathcal{B}_i} \cdot \vec{k}_b = J_r(\dot{r} + \varepsilon_i \dot{\omega}_i), \qquad i = 1, 2, 3, 4. \tag{11}
$$

To describe the orientation of the quadrotor we use the classical $\phi, \theta, \psi$ Euler angles (quaternions could of course be used). The direction cosine matrix $R_{\phi,\theta,\psi}$ to go from Earth coordinates to aircraft coordinates is then

$$
\begin{pmatrix} C\theta C\psi & C\theta S\psi & -S\theta \\ S\phi S\theta C\psi - C\phi S\psi & S\phi S\theta S\psi + C\phi C\psi & S\phi C\theta \\ C\phi S\theta C\psi + S\phi S\psi & C\phi S\theta S\psi - S\phi S\psi & C\phi C\theta \end{pmatrix},
$$

so that

$$
\vec{g} = g(-\vec{\imath}_b \sin\theta + \vec{\jmath}_b \sin\phi\cos\theta + \vec{k}_b \cos\phi\cos\theta). \tag{12}
$$

Finally the angles and angular velocities are linked by

$$
\dot{\phi} = p + \tan\theta(q\sin\phi + r\cos\phi) \tag{13}
$$

$$
\dot{\theta} = q\cos\phi - r\sin\phi \tag{14}
$$

$$
\dot{\psi} = \frac{q\sin\phi + r\cos\phi}{\cos\theta}. \tag{15}
$$

The thirteen equations (6)–(15) form the complete quadrotor model.

### C. Model of the inertial sensors

The quadrotor is equipped with strapdown triaxial gyroscope and accelerometer. Without restriction, we assume the sensing axes coincide with $\vec{\imath}_b, \vec{\jmath}_b, \vec{k}_b$. The gyroscope measures the angular velocity $\vec{\Omega}$, projected on its sensing axes, i.e. $(g_x, g_y, g_z) := (p, q, r)$; the accelerometer measures the specific acceleration $\vec{a} := \dot{\vec{V}}_P - \vec{g}$ of the point $P$ where it is located, projected on its sensing axe; see e.g. [18, chap. 4] for details on inertial sensors. Hence by (3) if the accelerometer is located at the center of mass $C$, which is the case for most quadrotors, it measures $\vec{a} = \dot{\vec{V}}_C - \vec{g} = \frac{1}{m}\sum_{i=1}^4 \vec{F}_i$; by (6) the accelerometer thus measures

$$
a_x := \vec{a} \cdot \vec{\imath}_b \qquad \approx -\frac{\lambda_1}{m}(\omega_1 + \omega_2 + \omega_3 + \omega_4)u \tag{16}
$$

$$
a_y := \vec{a} \cdot \vec{\jmath}_b \qquad \approx -\frac{\lambda_1}{m}(\omega_1 + \omega_2 + \omega_3 + \omega_4)v \tag{17}
$$

$$
a_z := \vec{a} \cdot \vec{k}_b \qquad \approx -\frac{a}{m}\left(\omega_1^2 + \omega_2^2 + \omega_3^2 + \omega_4^2\right). \tag{18}
$$

### D. Linearized model

To highlight the salient features of the revisited model (6)–(15), it is enough to consider its first-order approximation. Suitably putting together variables, this linearized model splits into four independent subsystems:

- longitudinal subsystem

$$
m\dot{u} \approx -mg\theta - 4\lambda_1\bar{\omega}u
$$
$$
\dot{\theta} \approx q
$$
$$
I\dot{q} \approx 4\mu_1'\bar{\omega}u - 4\mu_2''\bar{\omega}q + 2al\bar{\omega}(\omega_1 - \omega_3)
$$
$$
J_r(\dot{\omega}_1 - \dot{\omega}_3) \approx \Gamma_1 - \Gamma_3 - 2b\bar{\omega}(\omega_1 - \omega_3),
$$

with measurements $a_x \approx -\frac{4\lambda_1\bar{\omega}}{m}u$ and $g_y = q$

- lateral subsystem

$$
m\dot{v} \approx mg\phi - 4\lambda_1\bar{\omega}v
$$
$$
\dot{\phi} \approx p
$$
$$
I\dot{p} \approx -4\mu_1'\bar{\omega}v - 4\mu_2''\bar{\omega}p + 2al\bar{\omega}(\omega_4 - \omega_2)
$$
$$
J_r(\dot{\omega}_4 - \dot{\omega}_2) \approx \Gamma_4 - \Gamma_2 - 2b\bar{\omega}(\omega_4 - \omega_2),
$$

with measurements $a_y \approx -\frac{4\lambda_1\bar{\omega}}{m}v$ and $g_x = p$

- vertical subsystem

$$
m\dot{w} \approx -2a\bar{\omega}\left(\left(\sum_{i=1}^4 \omega_i\right) - 4\bar{\omega}\right)
$$
$$
J_r\left(\sum_{i=1}^4 \dot{\omega}_i\right) \approx \left(\sum_{i=1}^4 \Gamma_i\right) - 2b\bar{\omega}\left(\sum_{i=1}^4 \omega_i\right),
$$

with measurement $a_z \approx -g - \frac{2a\bar{\omega}}{m}\left(\sum_{i=1}^4 \omega_i\right)$

- heading subsystem

$$
\dot{\psi} \approx r
$$
$$
(J - 4J_r)\dot{r} \approx -\left(\sum_{i=1}^4 \varepsilon_i\Gamma_i\right) - 4\bar{w}\lambda_1 l^2 r
$$
$$
\left(\sum_{i=1}^4 \varepsilon_i\dot{\omega}_i\right) \approx \frac{J}{J_r(J - 4J_r)}\left(\sum_{i=1}^4 \varepsilon_i\Gamma_i\right)
$$
$$
- \frac{2b\bar{\omega}}{J_r}\left(\sum_{i=1}^4 \varepsilon_i\omega_i\right) + \frac{16\lambda_1\bar{\omega}l^2}{J - 4J_r}r,
$$

with measurement $g_z = r$.

In the sequel we concentrate on the longitudinal system, where accelerometer feedback is of paramount importance (the lateral subsystem is the same up to sign-reversing coordinate changes). Setting

$$
(f_1, f_2, f_3, f_4, f_5) := \left(\frac{4\lambda_1\bar{\omega}}{m}, \frac{4\mu_1'\bar{\omega}}{I}, \frac{4\mu_2''\bar{\omega}}{I}, \frac{2al\bar{\omega}}{I}, \frac{2b\bar{\omega}}{J_r}\right)
$$

and $\omega_q := \omega_1 - \omega_3$, $\Gamma_q := \frac{\Gamma_1 - \Gamma_3}{J_r}$, it reads

$$
\dot{u} = -f_1 u - g\theta \tag{19}
$$
$$
\dot{\theta} = q \tag{20}
$$
$$
\dot{q} = f_2 u - f_3 q + f_4\omega_q \tag{21}
$$
$$
\dot{\omega}_q = \Gamma_q - f_5\omega_q, \tag{22}
$$

with measurements $a_x = -f_1 u$ and $g_y = q$.

## E. Departure from literature

Most authors consider a propeller model with only the $\vec{k}_b$ terms in (1)-(2), i.e. with all $\lambda_i$'s and $\mu_i$'s equal to zero. They thus end up with the quadrotor model

$$m\dot{\vec{V}}_C = m\vec{g} - a\left(\omega_1^2 + \omega_2^2 + \omega_3^2 + \omega_4^2\right)\vec{k}_b \qquad (23)$$

$$\dot{\vec{\sigma}}_C = -b\left(\omega_1^2 - \omega_2^2 + \omega_3^2 - \omega_4^2\right)\vec{k}_b$$
$$+ al(\omega_1^2 - \omega_3^2)\vec{j}_b - al(\omega_2^2 - \omega_4^2)\vec{i}_b. \qquad (24)$$

Now a big problem should arise with such a model: indeed $\vec{a} = \dot{\vec{V}}_C - \vec{g}$ is now colinear with $\vec{k}_b$, hence $a_x = a_y = 0$, which is certainly not true! Without clearly acknowledging this paradox, the approximation $\vec{a} \approx -\vec{g}$ is used instead, i.e.

$$(a_x, a_y, a_z) \approx (g\sin\theta, -g\sin\phi\cos\theta, -g\cos\phi\cos\theta). \quad (25)$$

The alleged motivation is that $\dot{\vec{V}}_C$ is small near hovering. This is indeed true if the aircraft were stabilized by some extraneous means, but a very questionable assumption to use in a closed-loop perspective. Nevertheless, successful flights with controllers relying on this approximation have been reported. We suggest in section IV-C an explanation reconciling all those facts in the light of the revisited quadrotor model.

The longitudinal subsystem traditionally considered is then

$$\dot{u} = -g\theta \qquad (26)$$
$$\dot{\theta} = q \qquad (27)$$
$$\dot{q} = f_4\omega_q \qquad (28)$$
$$\dot{\omega}_q = \Gamma_q - f_5\omega_q, \qquad (29)$$

with measurements $a_x = g\theta$ and $g_y = q$, to be compared with (19)–(22) with measurements $a_x = -f_1 u$ and $g_y = q$.

## III. Experimental validation

### A. Experimental setup

To validate our modeling assumptions, we recorded flight data with our home-built "Quadricopter", see fig. 1. Due to limitations of our experimental setup, we could collect data to validate only the force model (19), but not the moment model (21); this is nevertheless the most important part of the model since it accounts for the accelerometer measurements. The quadrotor was fitted with a MIDG2 "GPS-aided Inertial Navigation System"[3] and a radio data link towards the ground station. The MIDG2 consists of a triaxial accelerometer, a triaxial gyroscope, a triaxial magnetometer, a GPS engine and an on-board computer. The raw measurements are "merged" on the onboard computer to provide estimates of the orientation and of the velocity vector in Earth axes. The MIDG2 is an "independent" device with no knowledge of the specific system it is fitted on; it heavily relies on the GPS engine for good dynamic estimates, without using assumption (25). All the data can be issued at a pace up to 20ms. Due to the low throughput of the radio data link, only the accelerometer raw measurements $a_{xm}, a_{ym}$ and the computed quantities $\phi_m, \theta_m, \psi_m$ and $V_x, V_y, V_z$
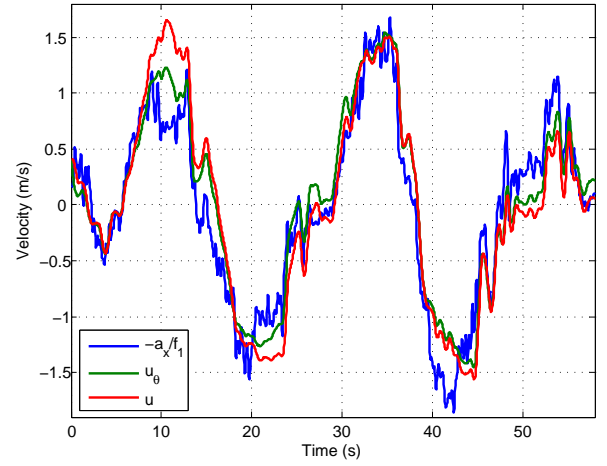
[3]www.microboticsinc.com



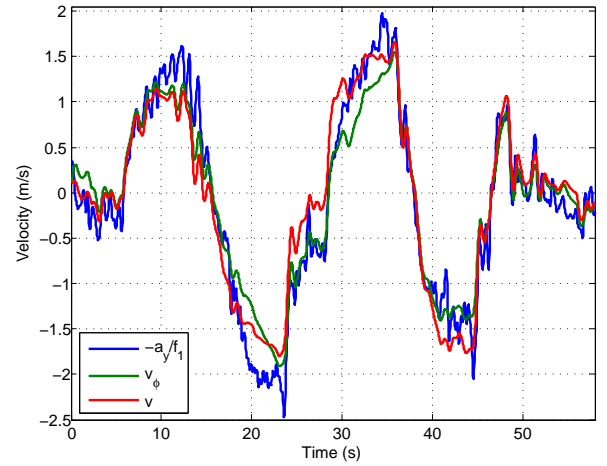Fig. 3. Comparison between $-\frac{a_x}{f_1}$, $u_\theta$ and $u$.



Fig. 4. Comparison between $-\frac{a_y}{f_1}$, $v_\phi$ and $v$.

were transmitted to the ground station, at the reduced pace of 40ms.

We flew the quadrotor in repeated back and forth translations at a (nearly) constant altitude and recorded one minute of flight data. Since a GPS module is used the test was conducted outdoors, on a very calm day to respect the no-wind assumption.

### B. Validation of the force model

Due to an imperfect mechanical design of our quadrotor, the MIDG2 case is not exactly aligned with the quadrotor frame, but tilted by the unknown (small) angles $\phi_0, \theta_0, \psi_0$. The acceleration and angle data must be rotated accordingly to be expressed in the quadrotor axes (the velocity data need not correction, since expressed in Earth axes), that is

$$(\phi, \theta, \psi) = (\phi_m - \phi_0, \theta_m - \theta_0, \psi_m - \psi_0)$$

and

$$\begin{pmatrix} a_x \\ a_y \\ a_z \end{pmatrix} = R^T_{\phi_0, \theta_0, \psi_0} \begin{pmatrix} a_{xm} \\ a_{ym} \\ a_{zm} \end{pmatrix}.$$
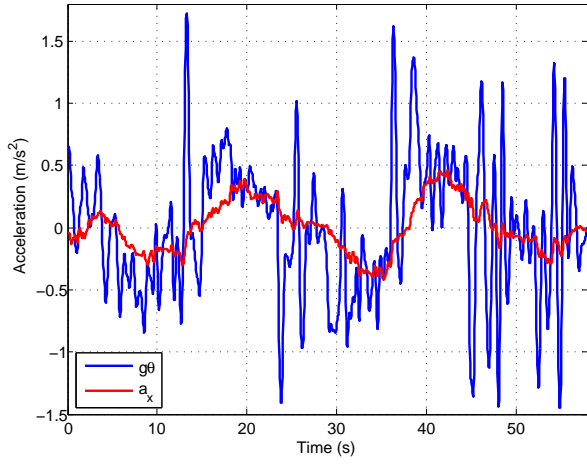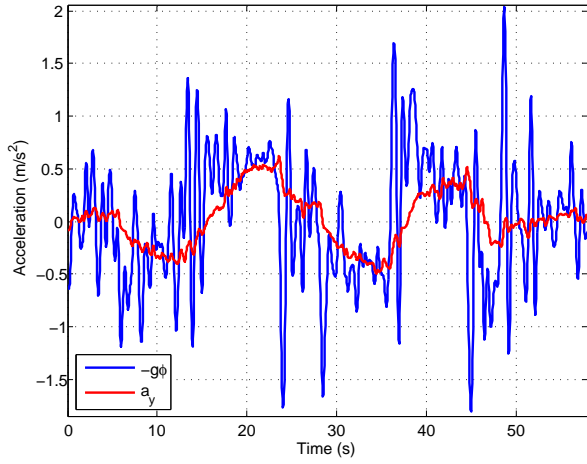
Fig. 5.   Comparison between $a_x$ and $g\theta$.



Fig. 6.   Comparison between $a_y$ and $-g\phi$.

Dropping higher-order terms, this yields

$$a_x \approx a_{xm} - \psi_0 a_{ym} + \theta_0 a_{zm} \qquad \approx a_{xm} - \theta_0 g$$
$$a_y \approx \psi_0 a_{xm} + a_{ym} - \phi_0 a_{zm} \qquad \approx a_{ym} + \phi_0 g.$$

The velocity vector in quadrotor axes is then obtained by

$$\begin{pmatrix} u \\ v \\ w \end{pmatrix} = R_{\phi,\theta,\psi} \begin{pmatrix} V_x \\ V_y \\ V_z \end{pmatrix},$$

and is considered as the "true" reference velocity to validate our modelling assumptions.

We also want to compute the velocities $u_\theta$ and $v_\phi$ predicted by the integration of the linearized force model (19)

$$\dot{u}_\theta = -f_1 u_\theta - g\theta$$
$$\dot{v}_\phi = -f_1 v_\phi + g\phi,$$

with initial conditions $u_\theta(0) := u(0)$ and $v_\phi(0) := v(0)$.

The task was then to adjust $f_1, \phi_0, \theta_0, \psi_0$ to get a good fit between $-\frac{a_x}{f_1}$, $u$ and $u_\theta$ on the one hand; and between $-\frac{a_y}{f_1}$, $v$ and $v_\phi$ on the other hand. Since the accelerometer data

are quite noisy and need some filtering, the same filter ($5^{th}$-order Bessel filter with 2Hz cutoff frequency) was applied to all the data to preserve the transfer functions among them.

With $(f_1, \phi_0, \theta_0, \psi_0) := (0.25\text{s}^{-1}, 1.2°, -2.4°, 2°)$ the agreement is good, see fig. 3 and 4, which reasonably validates our force model.

To test the traditional approximation (25) we also plotted $(a_x, g\theta)$ and $(a_y, -g\phi)$, see fig. 5 and 6. Though the trend is roughly correct, the fit is much worse.

## IV. IMPLICATIONS ON CONTROL SCHEMES

In the sequel we use the numerical values

$$(f_1, f_2, f_3, f_4, f_5) = (0.25, 0.76, -9.8, 0.34, 12.74);$$

$f_1$ was determined from flight tests, and $f_4, f_5$ from static tests on the motor-propeller subsystems. The aerodynamic coefficients $f_2, f_3$ were analytically derived; their values are plausible but nevertheless questionable.

### A. Two-time-scale "full-state" feedback

We first assume the whole state is known, or which turns out to be equivalent, that $u$ and $q$ are measured without noise so that they can be used in ideal Proportional-Derivative (PD) controllers. It is customary to design a two-time-scale control law, with a fast inner loop to control $q, \omega_q$ and a slow outer loop to control $u, \theta$.

The fast inner loop is the ideal PD controller

$$\Gamma_q = -\frac{k_p}{\varepsilon^2} q - \frac{k_d}{\varepsilon} \dot{q} + \frac{k_p}{\varepsilon^2} q_r,$$

where $q_r$ is the desired pitch rate; $k_p, k_d$ are the PD gains and $\varepsilon > 0$ is a "small" parameter. Applying this feedback to (19)-(22) yields

$$\dot{u} = -f_1 u - g\theta$$
$$\dot{\theta} = q$$
$$\varepsilon \dot{q} = f_4 \tilde{\omega}_q + \mathcal{O}(\varepsilon)$$
$$\varepsilon \dot{\tilde{\omega}}_q = -k_p q - f_4 k_d \tilde{\omega}_q + k_p q_r + \mathcal{O}(\varepsilon),$$

where $\tilde{\omega}_q := \varepsilon \omega_q$. From standard arguments of singular perturbations theory [20], the convergence of the fast variables is up to order $\varepsilon$ ruled by the well-known coefficient $f_4$ and the PD gains; and the behavior of the slow variables $u, \theta$ is up to order $\varepsilon$ ruled by the slow approximation

$$\dot{u} = -f_1 u - g\theta \qquad (30)$$
$$\dot{\theta} = q_r. \qquad (31)$$

Hence the role of the aerodynamic coefficients $f_2, f_3$ is marginal is the inner loop is fast enough.

The slow outer loop is the ideal PD controller

$$q_r = k_1 u + k_2 \dot{u} - k_1 u_r,$$

where $u_r$ is the desired velocity, and $k_1, k_2$ the PD gains. Applying this feedback to (30)-(31) yields

$$\dot{u} = -f_1 u - g\theta$$
$$\dot{\theta} = (k_1 - f_1 k_2)u - g k_2 \theta - k_1 u_r,$$

with characteristic polynomial $s^2 + (f_1 + gk_2)s + gk_1$. A reasonable closed-loop settling time is about $1s$, which requires $gk_1 = 6^2$ and $f_1 + gk_2 = 6\sqrt{2}$. This means $f_1 = 0.25$ is negligible w.r.t to the effect of the controller.

We thus see that the revisited moment model (21) does not rely matter if the gyroscope measurements are good enough for a fast loop, which is usually the case in practice; nevertheless taking into account $f_2$ and especially $f_3$ may help to design a better inner loop. As for the force model (19), it does not really matter either, provided a velocity measurement is available. The importance of $f_1$ is nevertheless paramount to account for the accelerometer measurements, as will be seen in the following sections.

### B. Traditional interpretation of accelerometer feedback

Once the inner loop closed, the traditional slow model is

$$\dot{u} = -g\theta$$
$$\dot{\theta} = q_r,$$

with measurement $a_x = g\theta$. Since the velocity $u$ is clearly not observable, the role of the outer loop is simply to control the measured angle $\theta$. In theory the simple proportional feedback $q_r = k(\theta_r - \frac{a_x}{g})$ does the trick, but in practice the accelerometer measurements are too noisy to be directly used (not only because of the intrinsic sensor noise, but also because of mechanical vibrations). Instead an "angle estimator" is often used, based on the model $\dot{\theta} = q$ with measurements $a_x = g\theta$ and $g_y = q$. A more elaborate estimator, e.g. an EKF or a nonlinear observer, can also be used, see the references in the introduction; it is then based on the nonlinear kinematic equations (13)–(15), and relies on the approximation (25). Whatever the filter, the first-order approximation is essentially the linear observer $\dot{\hat{\theta}} = g_y + l(\frac{a_x}{g} - \hat{\theta})$.

The outer loop thus is the controller-observer

$$q_r = k(\theta_r - \hat{\theta}) \tag{32}$$
$$\dot{\hat{\theta}} = q + l\left(\frac{a_x}{g} - \hat{\theta}\right). \tag{33}$$

Applied to the traditional model and defining the observation error $e_\theta := \hat{\theta} - \theta$, it yields the closed-loop system

$$\dot{u} = -g\theta$$
$$\dot{\theta} = k(\theta_r - \theta - e_\theta)$$
$$\dot{e}_\theta = -le_\theta.$$

For $\theta_r$ constant, the last two equations have the unique steady state $(\theta, e_\theta) = (\theta_r, 0)$. The characteristic polynomial is

$$\Delta_0 := (s + k)(s + l),$$

and the closed-loop transfer functions are

$$\theta = \frac{k}{s+k}\theta_r \tag{34}$$
$$u = \frac{-gk}{s(s+k)}\theta_r. \tag{35}$$

Provided $k, l > 0$ we have as desired $(\theta, e_\theta) \to (\theta_r, 0)$, while $u$ grows linearly unbounded. A good tuning of (32)-(33) requires for robustness that the controller and observer act in distinct time scales (Loop Transfer Recovery), i.e. $k \gg l$ or $l \gg k$. We consider in the sequel a "slow" observer, which is representative of commercial "angle sensors" such as the 3DM-GX, and a "fast" controller; for a settling time of about $1s$, we choose e.g. $k := \frac{1}{0.3}$ and $l := \frac{1}{12}$.

We tested this control scheme experimentally, with a rather satisfying result: the angle $\theta$ reaches the desired $\theta_r$, though the dynamics is somewhat more sluggish than expected. The traditional analysis could thus be considered as reasonably justified. Nevertheless it does not account for the following experimental observations already visible to the naked eye:

- when pushed away from hovering, the quadrotor returns to hovering (of course at a different position)
- when flying at a constant velocity $u$, the angle $\theta$ is not zero but approximately proportional to $u$
- in response to a constant $\theta_r$, $u$ does not grow unbounded but reaches a value approximately proportional to $\theta_r$.

Though these experimental facts are well-known to people in the field, they do not seem to be reported in the literature. The discrepancy is usually attributed to the neglected second-order aerodynamical drag and the inevitably unperfect experimental conditions. Another more subtle discrepancy is that the observer gain $l$ must be smaller than predicted by the theory to avoid a badly damped transient (e.g. $l = 1/3$ does not work well in practice).

As will be seen in the following section, these experimental facts can be explained by the revisited model.

### C. Revisited interpretation of accelerometer feedback

We now apply the controller-observer (32)-(33) to the revisited longitudinal model. The closed-loop system is now

$$\dot{u} = -f_1 u - g\theta$$
$$\dot{\theta} = k(\theta_r - \theta - e_\theta)$$
$$\dot{e}_\theta = -l\left(\frac{f_1}{g}u + \theta + e_\theta\right),$$

with $e_\theta := \hat{\theta} - \theta$. For $\theta_r$ constant, the only steady state is $(u, \theta, e_\theta) = (-\frac{g}{f_1}\theta_r, \theta_r, 0)$; the characteristic polynomial is

$$\Delta = s^3 + (k + l + f_1)s^2 + f_1(k + l)s + f_1 kl.$$

If $k \gg l$, $\Delta \simeq (s + k)(s^2 + f_1 s + f_1 l)$, so that the closed-loop system is stable as soon as $k, l > 0$. Hence $\theta \to \theta_r$ as desired, and $e_\theta \to 0$ as expected from the observer; $u$ now tends to the finite value $-\frac{g}{f_1}\theta_r$, which is more consistent with experimental tests. If moreover $l \ll f_1$,

$$\Delta \approx (s + f_1)(s + k)(s + l) = (s + f_1)\Delta_0.$$

As a consequence, the closed-loop transfer functions are

$$\theta = \frac{k(s + f_1)(s + l)}{\Delta}\theta_r \quad \approx \frac{k}{s + k}\theta_r$$
$$u = \frac{-gk(s + l)}{\Delta}\theta_r \quad \approx \frac{-gk}{(s + f_1)(s + k)}\theta_r,$$
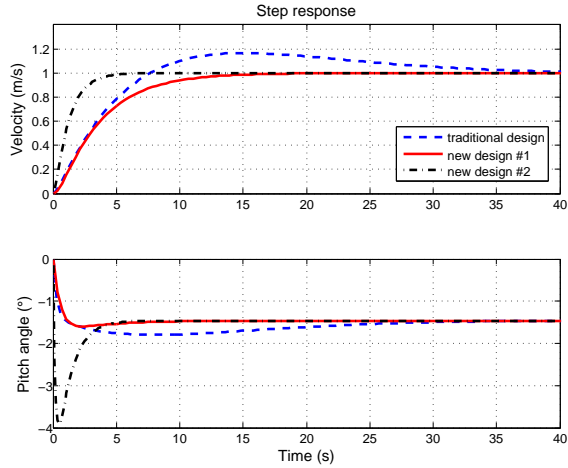
Fig. 7. Comparison between control schemes (simulation).

to be compared with (34)-(35): the angle dynamics is nearly the same as the one given by the traditional interpretation, while the velocity dynamics is dominated by the rotor drag time constant $\frac{1}{f_1}$. Defining the reference velocity $u_r := -\frac{g}{f_1}\theta_r$, we see the traditional control scheme, designed as an angle controller, is in fact a velocity controller!

The behavior experienced in practice is qualitatively and quantitatively well predicted by the revisited model, see fig. 7 ("traditional design") the time response to a $-1.5°$ step in $\theta_r$ (i.e. a $1m/s$ step in $u_r$).

From this analysis, we see the importance of the coefficient $f_1$ is paramount: the traditional scheme works reasonably well only because $f_1$ is positive and not too small.

*D. A better control law*

The performance of the traditional control scheme is limited by the rotor drag time constant $\frac{1}{f_1}$. Better performance can be achieved by considering a controller-observer based on the revisited model,

$$q_r = -k_1\hat{u} - k_2\hat{\theta} + \left(k_1 - \frac{f_1 k_2}{g}\right)u_r$$
$$\dot{\hat{u}} = -f_1\hat{u} - g\hat{\theta} + l_1(a_x + f_1\hat{u})$$
$$\dot{\hat{\theta}} = g_y + l_2(a_x + f_1\hat{u}),$$

where $u_r$ is the velocity reference; $k_1, k_2$ are the controller gains, $l_1, l_2$ the observer gains. Fig 7 shows simulation results for the same scenario as before ($1m/s$ reference step in velocity). Two different tunings were used: in the first case ("new design #1") the controller is tuned for a settling time of about $12s$ and the observer for about $48s$, so that the angle and velocity have initial transients similar to the tuning used previously for the traditional design (and with a similar control effort); in the second case ("new design #2") the controller is made four times faster.

Both design were successfully implemented, resulting in a quadrotor much easier to fly than with the traditional scheme. In practice it was not really possible to further

accelerate the time responses, probably mainly because the of accelerometer noise.

## V. CONCLUSION

We have proposed and experimentally verified a revisited model of the quadrotor. It is different, even at first-order, from the model traditionally considered in the literature. In particular it gives a different interpretation of accelerometer measurements. It explains why control schemes based on the traditional model nevertheless behave reasonably well, and should be useful to design better control laws.

## REFERENCES

[1] P. Castillo, A. Dzul, and R. Lozano, "Real-time stabilization and tracking of a four-rotor mini rotorcraft," *IEEE Transactions on Control Systems Technology*, vol. 12, no. 4, pp. 510–516, 2004.

[2] S. Bouabdallah, A. Noth, and R. Siegwart, "PID vs LQ control techniques applied to an indoor micro quadrotor," in *IEEE/RSJ Int. Conf. on Intelligent Robots and Systems*, vol. 3, 2004, pp. 2451–2456.

[3] A. Tayebi and S. McGilvray, "Attitude stabilization of a VTOL quadrotor aircraft," *IEEE Transactions on Control Systems Technology*, vol. 14, no. 3, pp. 562–571, 2006.

[4] P. Pounds, R. Mahony, and P. Corke, "Modelling and control of a quad-rotor robot," in *Australasian Conf. on Robotics and Automation*, 2006.

[5] N. Guenard, T. Hamel, and V. Moreau, "Dynamic modeling and intuitive control strategy for an "X4-flyer"," in *Int. Conf. on Control and Automation*, 2005, pp. 141–146.

[6] F. Kendoul, D. Lara, I. Fantoni-Coichot, and R. Lozano, "Real-time nonlinear embedded control for an autonomous quadrotor helicopter," *Journal of Guidance, Control, and Dynamics*, vol. 30, no. 4, pp. 1049–1061, 2007.

[7] S. Salazar-Cruz, J. Escareño, D. Lara, and R. Lozano, "Embedded control system for a four-rotor UAV," *International Journal of Adaptive Control and Signal Processing*, vol. 21, no. 2-3, pp. 189–204, 2007.

[8] G. Hoffmann, H. Huang, S. Waslander, and C. Tomlin, "Quadrotor helicopter flight dynamics and control: Theory and experiment," in *Collection of Technical Papers - AIAA Guidance, Navigation, and Control Conference 2007*, vol. 2, 2007, pp. 1670–1689.

[9] S. Bouabdallah and R. Siegwart, "Full control of a quadrotor," in *IEEE/RSJ Int. Conf. on Intelligent Robots and Systems*, 2007, pp. 153–158.

[10] N. Guenard, T. Hamel, and R. Mahony, "A practical visual servo control for an unmanned aerial vehicle," *IEEE Transactions on Robotics*, vol. 24, no. 2, pp. 331–340, 2008.

[11] A. Benallegue, A. Mokhtari, and L. Fridman, "High-order sliding-mode observer for a quadrotor UAV," *International Journal of Robust and Nonlinear Control*, vol. 18, no. 4-5, pp. 427–440, 2008.

[12] L. Derafa, T. Madani, and A. Benallegue, "Dynamic modelling and experimental identification of four rotors helicopter parameters," in *IEEE Int. Conf. on Industrial Technology*, 2006, pp. 1834–1839.

[13] T. Madani and A. Benallegue, "Backstepping control with exact 2-sliding mode estimation for a quadrotor unmanned aerial vehicle," in *IEEE/RSJ Int. Conf. on Intelligent Robots and Systems*, 2007, pp. 141–146.

[14] P.-J. Bristeau, P. Martin, E. Salaün, and N. Petit, "The role of propeller aerodynamics in the model of a quadrotor UAV," in *European Control Conf.*, 2009, pp. 683–688.

[15] R. Mahony, T. Hamel, and J.-M. Pflimlin, "Nonlinear complementary filters on the special orthogonal group," *IEEE Transactions on Automatic Control*, vol. 53, no. 5, pp. 1203–1218, 2008.

[16] P. Martin and E. Salaün, "Invariant observers for attitude and heading estimation from low-cost inertial and magnetic sensors," in *IEEE Conf. on Decision and Control*, 2007, pp. 1039–1045.

[17] ——, "Design and implementation of a low-cost attitude and heading nonlinear estimator," in *Int. Conf. on Informatics in Control, Automation and Robotics*, 2008, pp. 53–61.

[18] P. D. Groves, *Principles of GNSS, inertial, and multisensor integrated navigation systems*. Artech House, 2008.

[19] W. Johnson, *Helicopter Theory*. Princeton University Press, 1980.

[20] P. Kokotovic, H. K. Khalil, and J. O'Reilly, *Singular Perturbation Methods in Control: Analysis and Design*. SIAM, 1999.